Z. Phys. Chem. **219** (2005) 747–774

Review Paper

Fluorescence Imaging of Reactive Processes

By Clemens F. Kaminski*

Department of Chemical Engineering, University of Cambridge, New Museums Site, Pembroke Street, Cambridge, CB37BG, UK

This article is dedicated to Professor Marcus Aldén

(Received March 23, 2005; accepted April 13, 2005)

Laser Induced Fluorescence / Spectroscopic Imaging / Combustion Diagnostics / Biochemical Imaging / Microscopy

Laser induced fluorescence spectroscopy has emerged as the most powerful analytical tool to image reactive processes in a variety of systems. The purpose of the article is to review state-of-the-art example applications from a variety of research fields, which make use of LIF imaging for the visualisation of chemical reactions. Examples range from gas phase diagnostics of reacting flows to biomedical applications. There is a growing trend in the spectroscopy community to "work across disciplines" and one aim of this article is to highlight common principles behind seemingly unconnected research applications and to provide an incentive for spectroscopists to find novel application areas for their techniques and to point them to relevant literature.

1. Introduction

Fluorescence spectroscopy is one of the most versatile and sensitive tools in the analytical sciences to investigate the chemistry in technical and biological processes. One of the most powerful ways of deploying the technique is to illuminate molecular distributions in a plane and to image the resulting signals on 2D detection systems. This can be performed either by the simultaneous acquisition of multiple image elements on array detectors (static image acquisition), or, by the sequential scanning of an illumination point across the object plane and the reconstruction of the corresponding image information (dynamic image acquisition). Whatever method is used, the advent of the laser and of advanced detector technology, amongst which the CCD (charged

* E-mail: cfk23@cam.ac.uk

coupled device) is the most prominent, has led to a revolution in the field of fluorescence based imaging techniques, increasing their sensitivity and resolution beyond previous imagination. The technology is getting cheaper, better and more versatile, and at the same time the number of application fields is growing at an ever increasing rate. To some degree this has led to "split communities" amongst spectroscopists, because the application foci are becoming so specialised in the different disciplines that genuine communication barriers arise. However, change in circumstance – and interest – means that many spectroscopists are thinking actively about "discipline hopping" or are keen to find new applications for their methods. At first sight there may not appear to be much scope for transferring technology and know-how which is applied to visualise the chemistry in a gas turbine, to an application, which involves the investigation of chemical activity inside a living cell. However, for all their differences, there are many similarities in the two examples. At least one aim of the research is also the same: To deploy fluorescence imaging for obtaining insight into the spatial and temporal dynamics of chemical phenomena, including the formation of species, their destruction, and transport, and to link this information with other observations, *e.g.* whether an engine is running efficiently or whether a cell is dividing correctly. The purpose of this article is to review fluorescence based imaging techniques from this point of view and to contrast corresponding applications. Today one is mostly dealing with laser based excitation of fluorescence, *i.e.* laser induced fluorescence (LIF), and we shall confine our discussion to LIF on the understanding that, if non-laser excitation sources are used, appropriate overlap factors between the lineshapes of the source and the absorber are substituted in the calculations.

The article is structured as follows: First, a brief review is given on the theory of LIF, followed by a discussion of the principal mechanisms that affect LIF signals, with emphasis on the type of information that can be retrieved. Brief considerations are given to estimate signal strengths in representative applications, followed by a small number of examples for the the visualisation of reactive gas flows, and biochemical processes.

2. Principles of LIF imaging

The purpose of this section is to give a very brief summary of the most important theoretical considerations concerning LIF signal generation. There is a vast amount of primary literature on LIF experiment and theory. For in-depth coverage the reader should refer to some of the excellent textbooks that exist on the subject, for example [1–6]. Only key results will be stated here and emphasis will be given on common principles that apply across the range of examples given in this review. A unified presentation is attempted to avoid confusion which may arise from differing definitions applied in different re-

search fields (*e.g.* in gas phase spectroscopy and in fluorescence microscopy applications).

Laser induced fluorescence occurs upon the excitation of molecules from a lower energy level to a higher energy level by means of radiation emitted from a laser source. The molecules thus excited can give up some of their acquired energy by spontaneous emission of light and this constitutes the fluorescence signal. A LIF excitation spectrum is obtained by sweeping the laser wavelength across the molecular resonances and capturing the resulting fluorescence signals. Such a spectrum mimics an absorption spectrum of the investigated species and signal strengths depend on laser intensity, species concentration and temperature but also very much on the collisional environment the investigated species reside in.

LIF measurements can be obtained from a pointlike volume in space, for example by imaging the focal region of a laserbeam. The integrated LIF signal (in "signal units", for example Volts) is then given by

$$S = \underbrace{\frac{BI_{\mathrm{L}}\tau}{c}\Gamma}_{1}\ \underbrace{N_0 A_{\mathrm{L}} l f_{\mathrm{B}}}_{2}\ \underbrace{\Phi}_{3}\ \underbrace{\frac{\Omega}{4\pi}F_{\nu}\varepsilon\eta}_{4} \tag{1}$$

where B is the Einstein coefficient for stimulated absorption ($\mathrm{J\,m^3\,s^{-2}}$), I_{L} is the laser irradiance per unit frequency interval ($\mathrm{W\,m^{-2}\,Hz^{-1}}$), c is the speed of light, τ is the signal integration time (often the laser pulse length in pulsed laser applications), Γ is the spectral overlap of the laser lineshape with the absorption line profile, N_0 is the total number density of interrogated molecules ($\mathrm{cm^{-3}}$), A_{L} and l are the lateral and longitudinal extent of the interrogation volume ($\mathrm{cm^2}$ and cm, respectively), f_{B} is the Boltzmann population fraction in the lower energy state prior to excitation, Φ is the fluorescence quantum yield, F_{ν} is the fraction of total signal spectral bandwidth which is transmitted by the detection system, Ω represents the signal collection solid angle, ε is the transmission efficiency of the optical collection system, and η relates to the signal conversion efficiency (for example "V per signal photon"). Eq. (1) holds for fluorescence excitation in the linear regime (*i.e.* far away from saturation of the transition in question). The underbraced terms in Eq. (1) can be identified as follows: 1 refers to the excitation probability of individual molecules from the ground to the excited state, 2 is the total number of molecules in the interaction volume in the ground state prior to excitation, 3 denotes the fraction of excited state molecules which contribute to LIF signal as opposed to molecules which de-excite by other means, such as collisions, and finally 4 denotes the signal collection and photon-to-signal-conversion efficiencies. Collectively, terms 1, 2 and 3 denote the total number of fluorescence photons emitted from the interaction volume during the measurement time τ. The signal collection and conversion efficiencies have to be determined from a calibration experiment obtained from a known amount of analyte.

2.1 Fluorescence quenching

The most difficult term to account for in Eq. (1) is the fluorescence quantum yield Φ which depends on the collisional environment the molecules reside in. It is defined to be:

$$\Phi = \frac{A}{A+Q} \tag{2}$$

where A is the Einstein coefficient for spontaneous emission, denoting the number of molecules per second that contribute to LIF signal. Q is the rate at which excited state molecules are lost without having contributed to the LIF signal. This "loss of signal" is termed quenching. The excited state lifetime is given by:

$$\tau_{\mathrm{E}} = \frac{1}{A+Q} \tag{3}$$

which converges to the natural lifetime $\tau_{\mathrm{N}} = 1/A$ in the situation where $Q \ll A$. In the latter case the fluorescence quantum yield is near unity. Quenching can occur by many mechanisms including collisions, photodissociation and photoionisation, which produce nonfluorescent photoproducts, and interactions within the immediate matrix within which the analyte is embedded. Measurement of fluorescence lifetimes by LIF is a subject of increasing importance both for technical and biological applications, enabled by the availability of novel laser and detector technology, but this will not be discussed here.

For the purpose of this article, it is instructive to point to fundamental differences that exist between two application extremes and where the dominating mechanisms leading to quenching are different. These refer to measurements in the gas phase on the one hand, where low densities prevail and average distances between molecules are huge compared to molecular distances. On the other hand, in the liquid phase, analyte molecules are embedded in a matrix of solvent molecules and close range interactions may play an important role. The two cases are best illustrated by way of representative examples.

2.2 LIF in the gas phase

In the first example we consider an atmospheric pressure hydrocarbon fuelled flame at 2000 K in which OH radical concentration measurements are to be performed by LIF in the $A\,^2\Sigma - X\,^2\Pi$ electronic system, which has transitions near 305 nm. In the linear excitation regime (laser fluences below saturation values) the major contributor to quenching are molecular collisions with majority species (other species are too unlikely to be encountered by OH during its excited state lifetime for these to act as effective quenchers).

In the flame considered these will be N_2, H_2O, and O_2 and collisions with these species will lead both to rotational energy transfer (RET) [7], and to vibrational energy transfers (VET) [8], which change the shape of the fluorescence spectrum and lead to spectral shifts. A significant number of collisions will furthermore cause quenching: For the stated flame Q is of order $10^9\,s^{-1}$ compared to a spontaneous decay rate of A of $10^6\,s^{-1}$ for OH and thus there is a reduction in fluorescence quantum yield (= signal loss!) of order 10^3 compared to isolated OH molecules, which are not subject to collisions.

The collisions in flames are so energetic that new species may form with the target species, as relative velocities of colliding partners can exceed $2000\,ms^{-1}$. Apart from these inelastic collisions, which are the cause of quenching and energy transfer, elastic collisions may also take place. These disrupt the phase of emitted fluorescence signals and lead to line broadening (pressure broadening). For some small gas phase molecules of importance in atmospheric chemistry and reactive flow applications a computer code has been developed, which models the kinetics of the laser excitation and ensuing fluorescence processes in detail [9–11]. For excellent general reviews on this subject the reader is referred to [12] and [13].

Molecular rotation and collisions cause a reorientation of the excited state dipoles μ_e which are initially aligned with respect to the electric field vector of the excitation laser light. This leads to a depolarisation of the emitted fluorescence and is termed fluorescence anisotropy decay. In most gas phase environments this happens very quickly and anisotropies are destroyed on a ps timescale, although the effect may be noticeable [14, 15] and may even lead to errors in concentration or temperature measurements [16, 17]. In the liquid phase a similar effect happens, where its diagnostic potential is much greater, as will be discussed in Sect. 2.3.3.

2.3 LIF in solutions

The second example considers LIF of fluorophores in aqueous solutions. Such environments are frequently encountered in biomedical applications, for example during the visualisation of processes inside biological cells. Fluorophores used in such a context are often sensitive to quenching by molecular oxygen [18, 19] (and indeed, oxygen is a very effective quencher in the gas phase as well [20]). The likely mechanism is that molecular oxygen (which is paramagnetic) assists the process of intersystem crossing to the triplet state of the fluorophore, reducing fluorescence signals. What is the likelihood of a collisional encounter of a fluorophore with O_2 in such a situation? If oxygen transport is governed by diffusion, then the average distance Δx an oxygen molecule travels is given by Einstein's equation:

$$\Delta x^2 = 2D\tau \tag{4}$$

where D is the molecular diffusivity, and τ is the observation time [4]. Within a typical natural lifetime of emission of $\sim 10\,\text{ns}$ and a molecular diffusivity for O_2 in water of $D \sim 2.5 \times 10^{-5}\,\text{cm}^2\,\text{s}^{-1}$ this yields $\Delta x = 7\,\text{nm}$, which is of the order of the diameter of a single protein molecule or the thickness of a cell membrane! The corresponding molecular speed is of order of $\sim 1\,\text{ms}^{-1}$ and an important conclusion can be drawn when comparing this value to the previous example: In solution collisions are only likely with colliders within a molecular range of the fluorophore. LIF signals are therefore only affected by the very immediate vicinity of the fluorophore under investigation. This is very much in contrast to the high temperature gas phase example, where the signal is affected over more macroscopic domains, because of the high translational velocities prevailing. Furthermore, diffusive collisions in solution are generally too low in energy to drive chemical complex formation.

There are other mechanisms that lead to quenching in solution. Photodestruction ("photo bleaching") occurs frequently in biological microscopy [21], because of the high laser fluences achieved in the focal plane of high quality microscope objectives and the relatively long exposure times typically employed. Excited and ground state reactions and molecular rearrangements can occur, leading to non-fluorescing/non-absorbing species.

An important mechanism of excited state energy loss is non-radiative resonance energy transfer to species in close proximity. This mechanism does not involve photons for energy transfer and yet is – misleadingly – widely referred to as "Fluorescence Resonance Energy Transfer" (FRET) in the literature.

2.3.1 FRET

FRET occurs via a long range electrostatic dipole–dipole interaction between a so-called donor fluorophore, D, and an acceptor fluorophore, A, after excitation of D. For FRET to occur, the emission spectrum of D and the absorption spectrum of A must overlap. The rate of energy transfer is given by

$$k_{\text{FRET}} = \frac{1}{\tau_{\text{D}}} \left(\frac{R_0}{r} \right)^6 \tag{5}$$

where τ_{D} is the donor lifetime in the absence of A, r is the distance between the two fluorophores and R_0 is the Förster distance. Eq. (5) shows that at $r = R_0$, the rate of energy lost by D equals the rate of natural fluorescence emission $1/\tau_{\text{D}}$ in the absence of A. In other words, at the Förster distance, the rate of energy lost by FRET is equal to 50% of the total energy loss. D's fluorescence intensity then, would be diminished to half of that without A present. If A is a fluorescent molecule, then FRET transfer may be detected as "sensitised emission", *i.e.* A will start to fluoresce upon excitation of D if within $\sim R_0$ of D. R_0 is between 2 and 10 nm for fluorophore pairs of interest which is of the order of the size of biological macromolecules. FRET is therefore increas-

ingly becoming popular as a tool for measuring distances on the molecular scale and to obtain structural information on biomolecules. A precise quantification of the method is however difficult, as k_{FRET} depends on parameters such as the relative orientation of the donor and acceptor dipoles, the spectral emission and absorption profiles of D and A, and in biological systems one is often confronted with a distribution of distances giving rise to FRET signals and approximating assumptions have to be made. Förster's original publication on the theory of FRET [22] is highly readable (for the German speaking community!) and involves a semi-classical derivation of Eq. (5). An excellent, in-depth review on the theory of FRET, including quantum mechanical derivations and an English summary of Förster's seminal paper is given in [23].

FRET is increasingly becoming important for the verification of molecular binding events in biology, for example for the verification of protein–protein or enzyme–substrate interactions. The beauty of FRET is that it is a non intrusive measurement technique, which can be performed in live cells. The method usually requires the labelling of interaction partners with extrinsic fluorophores via molecular biology techniques and the "non-intrusiveness" depends on the degree to which the original functionality of the binding partners is conserved by this labelling. However, in contrast to FRET measurements for structural studies, here one is merely concerned with the question of whether FRET does or does not occur, signifying a molecular binding event or not. Even this seemingly much simpler task can be very difficult to perform in a live cell environment and artifacts may give rise to signals, which may be mistaken for a molecular interaction.

FRET is unlikely to occur in the gas phase where average distances between molecules are far too large. It is interesting to note, however, that in the gas phase a phenomenon of sensitised emission has also been observed, when using spectrally overlapping fluorescent tracer species [24, 25]. The phenomenon manifests itself in a similar fashion to FRET, although here the energy transfer is mediated by collisions, which are not required for FRET.

For biological macromolecules in solution FRET can be the major cause for fluorescence quenching. Although the spectral overlap requirement between D and A usually means that FRET is observed between different species (heteroFRET), the small Stokes shift of many biological fluorophores lead to a significant overlap between their absorption and emission spectra, such that at high fluorophore densities, significant signal quenching via FRET can occur (homoFRET). For example strong loading of biologically specific tags (*e.g.* an antibody) with fluorescein dyes may not lead to improved signals, as homoFRET occurs.

2.3.2 Solvent–fluorophore interactions

Other important differences exist in the solution phase compared to gas phase spectroscopy. Fluorophore–solvent interactions play a dominant role in shap-

ing the signal spectrum in the latter. The inducement of a dipole by the excitation laser causes solvent molecules in the vicinity of the absorber to reorient themselves. This effect is called solvent relaxation and occurs on timescales of 10^{-10} s. The energy expended during this process can result in very large Stokes shifts of the emission with respect to the excitation spectrum. Note that such reorientation effects do not play a role during absorption spectroscopy: The Franck–Condon principle [26] states that molecular motion is negligible during the timescale of photon absorption ($\sim 10^{-15}$ s, roughly the photon "transit time" across the absorber). Natural lifetimes in excited states are however very long (1 to 10 ns) compared to the solvent relaxation times (10 to 100 ps) and thus fluorescence can offer environmental information which absorption spectroscopy lacks [4].

2.3.3 Fluorescence anisotropy decays

Excited state dipoles μ_{E} will be preferentially oriented along the polarisation axis of the exciting light. If LIF were an instantaneous process (such as Rayleigh or Raman scattering nearly are), the emitted light would be perfectly polarised along the electric field vector of the exciting light. However, in the delay between excitation and emission there will be a significant number of collisions occurring which perturb this alignment process. For a small spherical molecule in a fluid of low viscosity one expects the ensuing fluorescence to be almost completely depolarised (isotropic). The rotational correlation time for a spherical molecule is given by

$$\theta = \frac{\eta V}{RT} \tag{6}$$

where η is the solvent viscosity, V is the volume of the rotating spherical molecule, R is the universal gas constant, and T is the temperature. Essentially the reorientation can be understood to result from a Brownian rotational diffusion. θ is the measure of how quickly a population of aligned dipoles adopts a random orientation as a result of this motion and is of order 100 ps to 10 ns for typical fluorophores in solution. This reorientation time is equivalent to the time in which the fluorescence emission decays from its initial fluorescence anisotropy value immediately after excitation to $1/\mathrm{e}$ of this value. These decays are strongly viscosity, fluorophore shape and size dependent, and thus offer diagnostic value: The anisotropy decays of a fluorescently labelled protein may change measurably depending on its folding state, the interaction with other proteins, or the binding to a membrane. This is in contrast to the gas phase, where anisotropy decays are usually too rapid to be of diagnostic value (see Sect. 2.2).

The effects so far discussed are illustrated on a Jablonski diagram shown in Fig. 1.

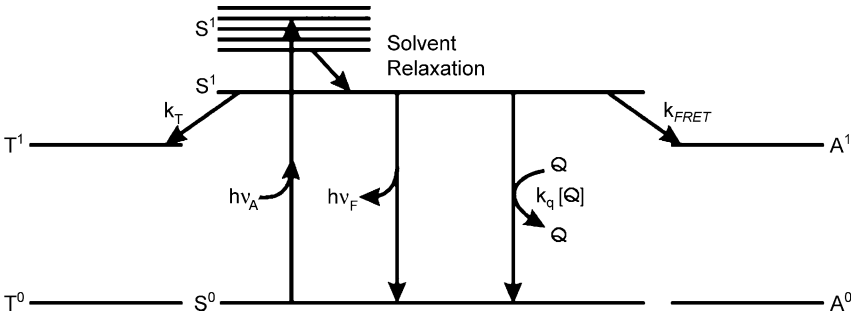

Fig. 1. Jablonski diagram illustrating various energy transfer processes in fluorophores. 0 denotes ground, 1 denotes excited states. S denotes singlet states, which are excited through absorption of photons at frequency ν_A, fluorescence is at frequency ν_f, depopulation by quenching occurs at rate $k_q\,[Q]$, where $[Q]$ is the concentration of quenching species, k_{FRET} denotes non-radiative transfer to acceptor molecules, k_T denotes transfer to triplet states.

3. Experimental considerations

One of the most powerful ways to employ LIF is by illuminating a cross sectional plane in the system of interest and to image the resulting signal such, that a 2D planar LIF image is obtained. This article focuses solely on such imaging applications. The technique allows one to resolve the fundamental relationships between structure and chemistry in the investigated processes. LIF thus deployed has revolutionised our understanding of complex reactive systems [27]. The way a flame burns in a turbulent flow field or how signals are transmitted inside living cells – our views on questions like these have been shaped by data obtained from LIF images.

3.1 Set-up for gas phase diagnostics

Fig. 2 shows a set-up commonly employed for LIF in the gas phase. The particular set-up shows an example where LIF is used to image the chemistry in a jet flame but the example is representative for a vast number of gas phase applications of LIF. The laserbeam is focused into a thin sheet of light, which traverses the flame. The fluorescence signal is captured at right angles and imaged onto a 2D array detector. Almost universally CCD (charge coupled devices) are used for LIF imaging today. Because of their importance both in the gas phase and in biological applications of LIF, these are given some consideration in the following section.

3.1.1 CCD cameras

CCD cameras are extremely sensitive devices with quantum efficiencies (photoelectrons produced per input photon) exceeding 90 % for top of the range

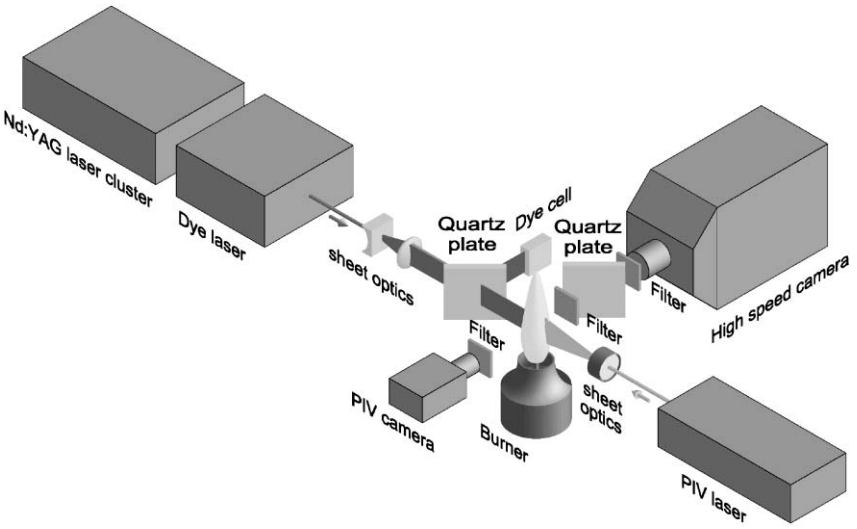

Fig. 2. Principle of planar light sheet imaging for flame diagnostics (PLIF stands for planar laser induced fluorescence). The PLIF system is used here in conjunction with a PIV (particle image velocimetry) system, which allows velocity field information to be recorded simultaneously with the PLIF signals. Laserbeam profile measurements are performed by passing a small fraction of the laser power through a homogeneous solution of dye, from which fluorescence is collected simultaneously with the PLIF flame signals. The particular set-up shown was used to perform the experiments in the turbulent flame described in Sect. 4.2, for which results are shown in Fig. 6. Adapted from Ref. [6] © Taylor and Francis.

back illuminated devices. They offer a high degree of linearity over dynamic ranges of 16 bit or more. Novel designs provide up to 10 million light sensitive elements, although there are tradeoffs with readout speed and dynamic range for very large chip sizes. High dynamic ranges and sensitivity require cooling to reduce dark current (thermally generated charge) and low charge readout speeds for high fidelity conversion into digital signals [28].

The bottleneck in CCD detection is readout noise which accumulates during the time the charge is amplified and read off the device (readout noise). This noise is largely independent of the amount of charge read out (but depends on the readout speed) and several technologies have been developed to amplify the signal before readout to increase the dynamic range. Image intensifiers are often used, which can increase the sensitivity of CCDs to the single photon level, comparable to, or better than photomultiplier devices (in fact, photomultipliers employing image intensifiers have recently entered the market). The intensifier consists of a photocathode, an electron conducting microchannel plate (MCP) and a phosphor screen and is situated before the CCD array. A very high voltage is applied across the microchannel structure and photocathode. Photons impinging on the photocathode will eject electrons

from the photocathode, which produce an avalanche of secondary electrons as these collide with the walls in the MCP device. The electron current is thus greatly amplified raising the signal well above the noise floor generated by the readout electronics. For low signal, short timescale applications the ICCD (intensified CCD) camera is the detector of choice: pulsing (or gating, as it is commonly called) the MCP voltage allows the device to be "shuttered" and exposure times as short as nanoseconds are routinely achieved. If a short signal pulse is to be detected against a luminous background, then the signal to noise ratio improves inversely proportional to the gate width, as long as all of the signal pulse is captured (*e.g.* an unintensified CCD with 10 ms exposure will collect 10^6 times as many noise photons as an ICCD camera gated for 10 ns). Disadvantages of ICCDs are their cost, susceptibility to damage when exposed to high light levels, and a loss of resolution compared to unintensified CCDs.

Other technologies are entering the market now, such as electron bombardment CCDs (ECCDs) and on chip multiplication gain devices [28–30]. The latter are especially promising: Here signal amplification is produced directly in the chip's readout register (before the charge enters the charge readout amplifier) exploiting the phenomenon of impact ionisation. The latter creates secondary charges in a CCD pixel, upon application of a large voltage. In contrast to ICCD devices the risk of damage is low for these systems and on chip signal gains of 1000 can be achieved.

The framing rate of high quality CCD cameras is limited by the readout process (tens of ms to several seconds, depending on required quality and chip size). A problem with this is that during readout, the chip must not be exposed to light and readout must be completed before the next exposure takes place. This limits frame rates to several frames a second at most. So-called frame transfer technology overcomes this problem by dividing the CCD area into a light sensitive area and an equal area adjacent to it which is used for temporary storage of the charge. The storage area is coated with an opaque layer, and charge from the light sensitive portion is continuously shifted over to the storage part, from where it is read off. The advantage is that while the signal is integrated on the the light sensitive part of the chip, the information from the storage area can be read out. Framing rates of several 100 per second (on limited pixel areas) are possible using this technology, but a disadvantage is that some image smearing can occur during frame transfer. Recently interline transfer cameras have entered the market, which overcome this problem, but these suffer decreased photosensitivity, and dynamic range.

3.1.2 Spatial resolution and signal levels

How many photons are generated in a typical PLIF situation and what fraction reaches the individual pixel elements on the imaging device? It is instructive

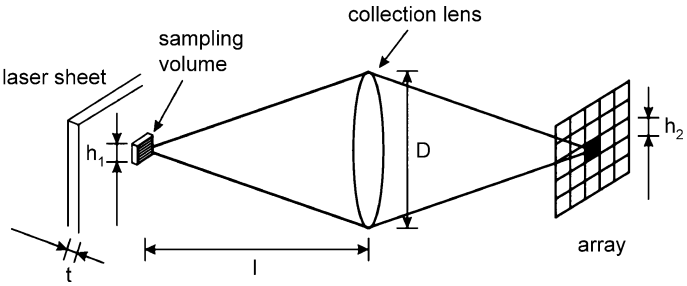

Fig. 3. LIF signal collection from a laser sheet. The magnification is $M = h_2/h_1$, the sheet thickness is given by t, the collection f-number is given by $f_\sharp = D/l$.

Table 1. Conditions for the example PLIF application discussed in Sect. 3.1.2. The corresponding imaging geometry is shown in Fig. 3.

quantity	explanations
$n = 0.05\%$	OH mole fraction
$T = 2400\,\mathrm{K}$	flame temperature
$\tau = 10\,\mathrm{ns}$	laser pulse duration
$t = 0.5\,\mathrm{mm}$	laser sheet thickness
$I = 0.3\,\mathrm{W\,m^{-2}\,Hz^{-1}}$	laser irradiance
$N = 500^2$	number of pixel elements on ICCD
$(h_2)^2 = 20\,\mu\mathrm{m}^2$	area per pixel element
$M = 0.2$	optical magnification
$f_\sharp = 1/4$	f-number of signal collection optics
$B = 5 \times 10^{18}\,\mathrm{J^{-1}\,m^3\,s^{-2}}$	Einstein absorption coefficient for selected OH transition
$\phi = 3 \times 10^{-3}$	fluorescence quantum yield of selected transition

to consider as an example a turbulent flame (*e.g.* as shown in Fig. 2) in which one wishes to image the distribution of the OH radical, which is chemically produced in the reaction zone of the flame and convects with the hot combustion products. The OH radicals are assumed to be at 2400 K, at a mole fraction of 0.05%, representative of many lean hydrocarbon fuelled flames. The laser is focused to a sheet, 0.5 mm in thickness and imaged with $f_\sharp = 1/4$ onto an ICCD device with a demagnification of $M = 0.2$ between object and image (as would be obtained, for example, by imaging a $50 \times 50\,\mathrm{mm}^2$ flame region onto a $10 \times 10\,\mathrm{mm}^2$ chip). Fig. 3 shows the imaging geometry and Table 1 states the conditions of the measurement. What is the number of photons striking each detector element (pixel)? In the example we assume that Γ in Eq. (1) is near 1 and that the laser irradiance is close to the saturation intensity of the transi-

tion, which, as a rule of thumb, ensures an optimal signal-to-noise ratio. The result is that around 3×10^5 photons are incident onto each pixel during the signal pulse. In contrast, the imaged volume per image pixel contains of order 10^{10} OH molecules in the probed quantum level and thus on average only about 1 in 10^5 will contribute a signal photon during the pulse. The photon shotnoise is given by:

$$F_{\mathrm{SN}} = \sqrt{N} \tag{7}$$

where N average photon flux in the signal. It represents the fundamental limit in the achievable signal to noise ratio and in the current example this would only amount to around 0.2%, which is likely to be negligible compared to other sources of noise. More signal is obtainable by increasing the laser power, but not necessarily at improved signal to noise levels: Above saturation intensities signal powers level out, whilst background levels (*e.g.* from particulate scattering and reflections of optical components) continue to increase linearly.

3.2 Microscopic LIF imaging

In biological applications one is often faced with the problem of having to excite and collect fluorescence over very small volumes. Examples range from DNA sequencing in microcapillaries to the imaging of living cells. The linear dimensions of a single mammalian cell, for example, are of the order of 10 μm, and clearly different imaging strategies than those used in combustion research need to be adopted to obtain fluorescence signals from subcellular components or intracellular events. In a fluorescence microscope sophisticated condenser optics are used to illuminate the sample and the signals are collected with high quality microscope objectives. The highest resolution instruments are confocal microscopes, where a high power objective is used both as a condenser for laser illumination, and for collecting the (Stokes shifted) signal light. The lateral resolution obtainable with a confocal microscope is similar to a conventional fluorescence microscope (of order of the wavelength of the light used to illuminate the sample), but the great advantage of the instrument is that signals from out of focus illumination planes in the sample are rejected by placing a pinhole in the image plane of the illumination focus (confocal plane). Thus signals are only received from a well defined point in the sample. A 2D image is built up by scanning the laser focus along x and y. Recording several xy sections in different z planes allows full three-dimensional information to be recovered. A setup for a so-called confocal laser scanning microscope (CLSM) is shown in Fig. 4. The lateral resolution of the image is limited by diffraction and can be calculated by considering the diffraction pattern formed in the image plane of the objective upon imaging an infinitesimally small emitter. This yields the point spread function (PSF) [31, 32]. The first minimum

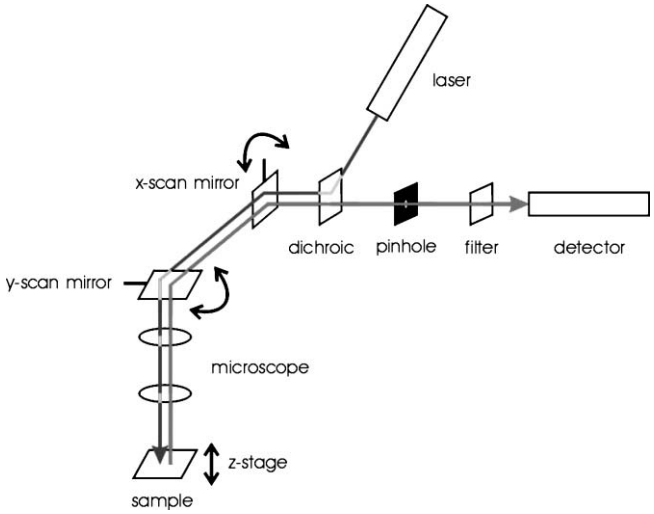

Fig. 4. Principle of confocal laser scanning fluorescence microscopy.

of the resulting circular diffraction pattern for a diffraction limited system is given by

$$r = 0.6\frac{\lambda}{NA} \tag{8}$$

where λ is the fluorescence wavelength and NA is the numerical aperture of the objective lens. NA is given by

$$NA = n\sin(\alpha) \tag{9}$$

where n is the refractive index of the medium between lens and sample and α is the half angle of the cone of light accepted by the objective from the measurement point. Good instruments can achieve resolutions of the order of the excitation wavelength. It is clear that NA is related to the light gathering power of the instrument and therefore related directly to $f_\#$ in the previous example and Ω in Eq. (1). For good quality systems this cone half angle may be greater than 65 degrees corresponding to $\sigma/4\pi = 0.3$, which corresponds to nearly 80 times the collection efficiency compared to the previous example for PLIF. As a representative example a system is considered here with $NA = 1.2$, 488 nm laser excitation and fluorescein as the species to be detected in a biological environment (fluorescein is a popular dye label in biology because of its photostability and relative independence of fluorescence characteristics on environmental conditions). Table 2 states the conditions for this case. The illumination spot size for this system is around 500 nm in diameter. For a 500 μW laser this results in an irradiance of 2.5×10^{24} photons per second per square

Table 2. Conditions for the microscopic measurement discussed in Sect. 3.2 with a set-up as shown in Fig. 4.

quantity	explanations
$NA = 1.2$	numerical aperture of objective
$I = 500\,\mu\text{W}$	excitation power
$\lambda = 488\,\text{nm}$	excitation wavelength
$\phi = 0.9$	quantum efficiency of fluorescein
$Q_{\text{ISC}} = 0.03$	quantum efficiency of singlet to triplet transfer
$\tau_{\text{F}} = 4.5\,\text{ns}$	upper state fluorescence lifetime
$\tau_{\text{T}} = 1\,\mu\text{s}$	triplet state lifetime
$\sigma = 3 \times 10^{-16}\,\text{cm}^2$	absorption cross section per molecule
$N = 512 \times 512$	number of image pixels
$t = 0.25$ seconds	time required to acquire one image

cm. For the given absorption cross section σ of fluorescein at 488 nm excitation this results in an absorption rate of $k_{\text{a}} = \sigma I = 1.5 \times 10^8\,\text{s}^{-1}$, which is close to the fluorescence rate $k_{\text{F}} = 1/\tau_{\text{F}} = 2 \times 10^8\,\text{s}^{-1}$ (consult [33] for an excellent review of the relationships between absorption cross-sections, *B*-coefficients etc.). In other words significant population will be in the excited state ($\sim 40\%$) for this laser irradiance and therefore the signal is strongly saturated. Increases in laser power do not contribute significantly to extra signal, whilst raising the noise floor. In the liquid phase, background due to Rayleigh and Raman scattering are substantial because of the much larger densities compared to the gas phase example. A further important distinction is the sequential mode of image acquisition: If it takes 0.25 seconds to scan a 512×512 pixel image, the laser dwell time is around 1 μs per pixel. On this timescale there is a significant probability of intersystem crossing (from the singlet excited state to the spin forbidden, and thus long lived, triplet state). If the quantum efficiency Q_{isc} for this intersystem crossing is 0.03 ([34]) and the lifetime of the triplet state is 1 μs then it takes only a few 100 ns until equilibrium is reached between singlet ground, singlet excited and triplet excited states for the above pumping rates. This will result in relative populations of 10, 20 and 70 percent respectively in these three states and thus very significant signal loss [4]. The risk for photodamage is also greatly increased, especially if *z*-sectioning is performed: Whilst the signal photons from out of focus planes are effectively rejected by the pin hole, these planes are still subject to laser illumination.

A quantitative calculation regarding obtained signal levels is difficult given the uncertainty in the various listed quantities (the triplet state lifetime, for example, can vary orders of magnitude with oxygen concentration) but for the stated conditions every fluorophore will emit thousands of fluorescence pho-

tons per pixel acquisition time. Of these only a few will make it through to the detector, as signal transmission losses are very high in a microscope because of the large number of intermediate optical components and the confocal pinhole. Nevertheless, one clearly sees, that there is a vast difference compared to the gas phase spectroscopy example in the contribution individual molecules make to the signal.

4. Examples: gas phase chemistry

The following section shows examples from a range of applications, where fluorescence imaging has been used to explore the spatio-temporal dynamics of reactive systems. There is a huge range of literature on such topics and necessarily this review is biased towards applications that are of research interest to the author. The main aim here is to contrast a few applications, which employ LIF to look at processes on the macroscopic scale on the one hand with those, that occur on a microscopic scale on the other, and, hopefully, to instill some interest in researchers who are keen to look "across disciplines". In all examples the focus is on the visualisation of dynamic, reactive systems although on very differing spatial and temporal scales.

4.1 Reaction rate imaging

The first example concerns the application of PLIF for the visualisation of local reaction rates in a turbulent flame. A key question in combustion research is the definition and localisation of the reaction zone where exothermic reactions release heat. These zones may be very thin (a typical flame front in a technical combustion process is of sub-millimeter dimensions) and the way a flame propagates depends crucially on the behaviour of the flame front when it is subjected to convective stresses and heat loss by mass diffusion and radiation. In hydrocarbon flames, the local concentration of the formyl radical, HCO, is an excellent indicator of the flame front: The reaction pathways leading to HCO production account for 30 to 40% of the flame's heat release rate and since this radical is extremely short lived (ns), its local concentration is a direct measure of local heat release rates. However, imaging HCO directly by PLIF is an almost impossible task for dynamic flow systems, owing to the very low signal strengths obtained which would require temporal averaging over many laser shots for useful signal to noise ratios to be obtained. This destroys any dynamic information from the flow, and thus a different approach has been adopted, which is based on the simultaneous imaging of formaldehyde (CH_2O) and OH radicals [35, 36], which take part in the reaction:

$$CH_2O + OH \rightarrow HCO + H_2O\,. \tag{10}$$

It is possible to select transition lines for OH and CH_2O, such that the product of their respective signals depends on temperature and local mixture fraction

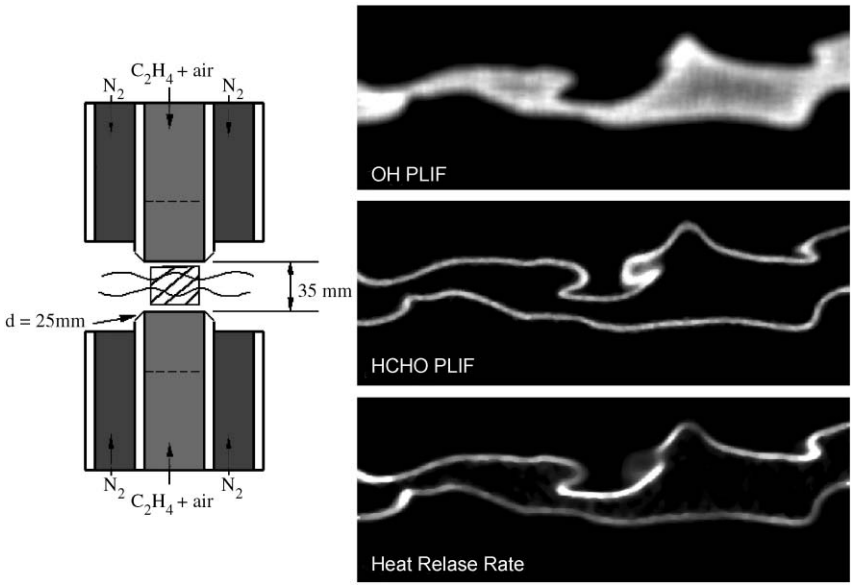

Fig. 5. Reaction rate imaging in an opposed premixed jet flame. The left hand side shows the experimental set up. Two shaped nozzles are arranged in opposing fashion and eject turbulent streams of ethylene and air. When ignited, a double fronted flame structure is established as indicated. A coflow of N_2 in both streams is used to protect the flame from entraining laboratory air. The shaded region corresponds to the imaged regions on the right. On the right hand side signals are shown from OH (top), CH_2O (middle), and the product image which correlates with heat release rate. Strong heat release rates (*i.e.* regions where HCO production is high) are observed in regions which are strongly curved, but note that there is a highly curved vortical structure in the CH_2O image, which has no corresponding feature in the OH image. Here the product image exhibits very little signal, indicating that reactions have (or are about to become) extinguished. Image dimensions are 41 mm by 15 mm. Flame fronts are less than 1 mm in thickness.

in a similar way to the forward reaction rate k_f of the above reaction. As HCO is consumed very quickly after its formation by reactions, k_f is an excellent indicator of HCO concentration itself.

Fig. 5 shows an application of this technique in a turbulent counterflow premixed flame. Two nozzles ejecting ethylene and air are opposing one another and the streams meet in a stagnation zone situated somewhere between the two nozzles. The configuration leads to a double flame structure. OH is formed close to the reaction zone and convects towards the stagnation plane, filling the gap between the two flame fronts. The CH_2O images in turn are located close to the reaction zones which are visualised by the heat release (HR) image (the product image of OH and CH_2O). Several features are noticeable on the HR image: The heat release rates are highest in regions that are negatively curved (*i.e.* concave) towards the oncoming reactant streams. This is a manifestation

of a complex interplay between thermal and mass diffusion, the relative importance of which is given by the Lewis number (essentially the ratio of thermal to mass diffusion timescales). For flames with Lewis numbers less than 1, as is the case for the present example, diffusion across flame fronts which are concave lead to a concentration of light and highly reactive species such as H atoms in regions immediately upstream of these concave features [37–39]. This in turn speeds up local reaction rates and thus an increase in heat release rates results. It can furthermore be seen that there is a vortical feature on the CH_2O image, which has no corresponding feature in the OH images. The product signal in this region is therefore close to zero, indicating a break in the reaction layer. Such data is instrumental in the development of our understanding of the complex interplay between turbulent flow fields and flame propagation and is used in the development of numerical models and theoretical descriptions of complex reacting flows. Heat release fluctuations in technical combustion systems lead to instabilities, with detrimental effects on pollutant emissions, and engine stability: Only now is it possible to visualise these complex and delicate phenomena in a direct fashion.

4.2 Turbulence/chemistry interactions

Phenomena of the type shown in the previous section stem from interactions of turbulent flow features with the flame front. As discussed, such turbulence/chemistry interactions affect burning rate and flame stability. For example, excessive strain can cause a thinning of the reaction zone, which in turn leads to increased heat loss by diffusion. The flame chemistry responds to this with deviations from equilibrium and eventually extinguishes if exposed to high strain rates for a sufficiently long time. The study of flame-turbulence interactions is fundamental in the construction of models of technical combustion systems, because both flame burning rate and stability are affected by such interactions [40]. Turbulence/chemistry interactions are however notoriously difficult to study directly, because of the very small temporal and spatial scales over which such phenomena occur. In combination with flow field measurements, the sequential acquisition of PLIF images allows one to correlate flame structural information with local strain rates and this is probably the most powerful way of obtaining an insight into such phenomena. In Fig. 6 the principle of such a measurement is shown, performed in the turbulent jet flame depicted on the lower left hand side of the figure (Reynolds number $\mathrm{Re} = 22\,800$ based on exit velocity, nozzle exit diameter: 8 mm, [41]). Measurements were performed by time sequencing PLIF measurements at 30 μs intervals and conducting a simultaneous PIV measurement of the gas flow velocity field. The set-up for this experiment corresponds to that in Fig. 2. The flame runs on a mixture of CH_4, H_2 and N_2, which emanates from the central tube, surrounded by a slower flow of air. The two gas streams form a shear layer between them and a diffusion flame is established which is stabilised close to

the nozzle rim. The flame is imaged in the region shown by the rectangular box in Fig. 6b. The sequence of OH images shows clearly a region where the flame front thins and extinguishes. The reason for this becomes apparent by investigation of the simultaneously obtained strain rate field (from PIV measurements). Several things are noticeable from the last image of the sequence, which shows the strain rate field and the OH contours superimposed. The maximum strain rates occur in regions just to the inside (the fuel rich side) of the flame front, where turbulence levels in the jet are highest. In most regions defined by the OH contours the flow is seen to be laminarised because of the the higher viscosity of the burnt gases (the kinematic viscosity changes by a factor of 15 from unburnt to burnt gases), leading to low turbulence levels and strain rates. In the region marked as A, however, strain rates are seen to be abnormally high in the flame front, leading to flame front thinning and subsequent extinction of reactions (seen clearly on inset c). The flame front becomes thinner, which results in stronger gradients and thus greater loss of reactive species and heat by diffusion, which close to extinction is greater than the heat released by flame reactions. Such data is ideally suited for comparisons with results from numerical modelling activities [42] and helps to form a better understanding of the underlying phenomena. LIF, like no other technique, has led to vastly improved capabilities for the development of models and the description of turbulent flow fields with chemistry [6]. More and more applications of LIF are aiding in the design of more efficient and less pollutant engine technology both directly, by providing engineers with practical insight into the devices they develop, and indirectly, by improving our fundamental understanding of the physics and chemistry of complex reacting gas flows.

5. Examples: biological applications

The role of fluorescence spectroscopy for the investigation of reactions in biological applications has never been more dominating than today. With the genomic sequences of many organisms resolved, a huge global effort is now underway to correlate genetic information with the underlying function of proteins in living cells. A major breakthrough in this effort has been the development of fluorescent *in situ* protein labelling techniques. With variants of the so-called green fluorescent protein (GFP), derived from the jellyfish Aequorea Victora, it is now possible to selectively label individual proteins in the living cell without corruption of their function [43, 44]. The fluorescent protein (FP) was derived from a single gene in the mentioned jellyfish and, remarkably, the gene could be expressed in non jellyfish organisms without loss of its fluorescent properties. Several mutants have been produced of the original gene, yielding proteins of improved brightness, photostability and a reduced susceptibility to environmental effects, such as pH and quenching. Furthermore, a whole spectrum of colours is now available, spanning the entire visible

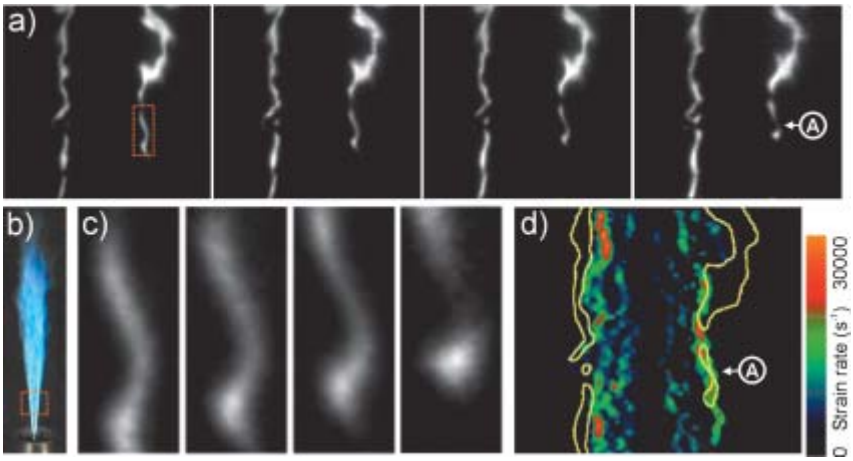

Fig. 6. Time resolved PLIF imaging of turbulence chemistry interactions. a) Sequence of 4 PLIF images of OH, obtained at 30 μs time intervals. The indicated region shows clearly how the flame front is thinning in time. Image dimensions correspond to 32 by 31 mm^2. The rectangular box indicates the region which is shown magnified in c). b) Photograph of flame with imaged region superimposed. The rectangular box corresponds to the region shown in a). c) Magnified image of the region, in which a localised extinction event is occurring: The flame front is clearly thinning and finally extinguishes. d) Corresponding strain rate field obtained from simultaneously performed PIV measurements. It can be seen that the strain rate values are high within the flame front (superimposed as a yellow contour), which is in contrast to other regions in the flame, where the maximal strain rates are towards the centre of the jet, away from the flame front. The image is taken from Ref. [42] © The Combustion Institute 2005.

range and permitting the specific and highly selective labelling and imaging of multiple entities within the same cell [45]. Proteins of interest are labelled by fusing their genes with the gene of the desired FP label, thus yielding a fusion protein construct containing the fluorescent marker. Almost any cell type can express the labelled protein chimeras without loss of function and this remarkable phenomenon has become one of the most important tools of modern biology. Using FP labelling and fluorescence microscopy, imaging of the function, interaction, localisation, expression and degradation of proteins can be studied directly at the living cell level. In the present context two examples will be reviewed to visualise intracellular reactions and transport of FP-labelled proteins.

5.1 Protein mobility in live cells

Important questions relating to protein function relate to the localisation and mobility of specific proteins in the live cell. Are the proteins confined to certain compartments inside the cell, or are they free to move from one location

to another by diffusive transport? Is molecular transport enhanced by machinery internal to the cell and is it a function of the state of the cell during its cycle? A powerful tool has recently emerged to provide answers to such questions, known as FRAP (fluorescence recovery after photobleaching) [46]. The principle is to use an intense, localised laserbeam to selectively photobleach a population of fluorescently labelled fusion proteins in a small area of the cell, followed by the observation of the fluorescence signal rise as the bleached region is filled up again by non-bleached fluorescent molecules. The speed of this fluorescence recovery (recorded at low excitation power to prevent further bleaching), is a measure of the proteins' mobility. In the absence of any active transport within the cell, the characteristic timescale τ_d of recovery is determined by Brownian motion and is inversely proportional to the diffusion coefficient D. For two-dimensional diffusion into a circular area of width ω (defined by the $1/e^2$ intensity points in the focus of the bleaching laser) this can be expressed as [47]:

$$\tau_d = \omega^2 \gamma / 4D \tag{11}$$

where γ is a factor to account for incomplete bleaching. This equation assumes that diffusion is unobstructed in two dimensions, that the bleached spot is circular in area, and that no diffusion takes place along the axis of the laserbeam (*i.e.* bleaching is uniform along the laser line). It represents a reasonable approximation for proteins which diffuse along membranes (*e.g.* cell walls) but probably oversimplifies the problem for other cases [48]. The diffusivity D in turn is related to temperature T and the viscosity of the surrounding medium μ as:

$$D \propto T/\mu R_h \tag{12}$$

where R_h is the hydrodynamic radius of the diffusing protein. Significant deviations from free diffusion can occur, when there are interactions of the protein with other proteins or collisions with cytoskeletal filaments. In membranes, diffusion is very much slower than that of proteins moving freely in the cell interior, due to the much higher viscosity of (lipid) membranes. An example of FRAP and the dynamics of protein mobility inside live cells is shown in Fig. 7. The example shows the use of FRAP to verify an increased motility of the Plk1 (polo-kinase 1) protein as the cell is going through mitosis (cell division). Plk1 is a major regulator of the cell cycle and in the example shown it is visualised by a yellow variant of GFP (YFP – yellow fluorescent protein). The image sequence shows Plk1 concentrations in a live human cell in its early stages of division at four different time points. For each stage shown, three pictures are presented: The first shows the cell before the bleaching laser has been turned on, the second is taken immediately after the bleaching laser has been switched on, and the third shows the cell after fluorescence recovery. Arrows mark the focus of the bleaching laser in which the fluorphores are

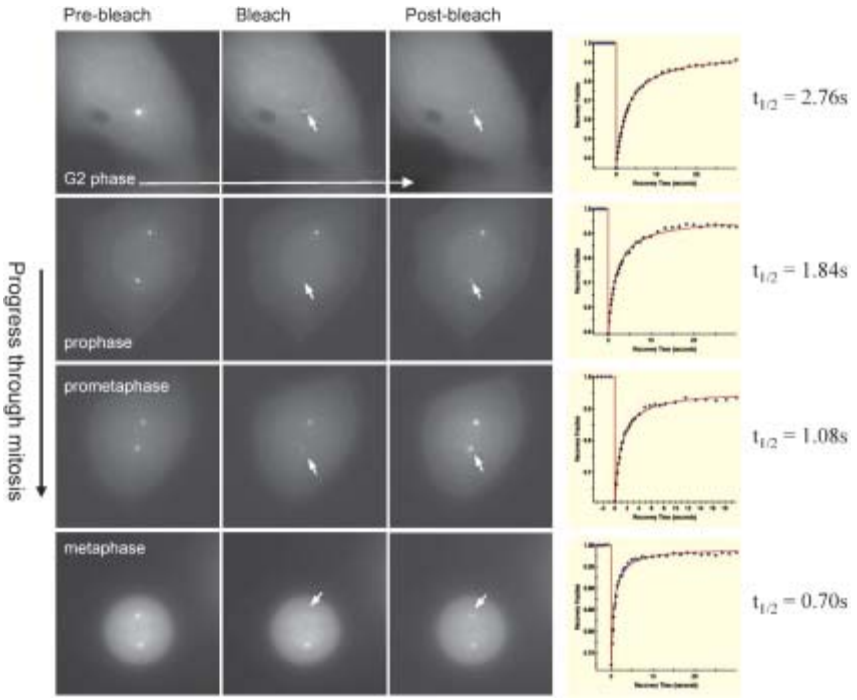

Fig. 7. Using FRAP to examine the dynamics of a major cell cycle regulator, polo-like kinase 1 (Plk1) during cell division (mitosis). YFP-tagged Plk1 at the microtubule-organising centre (MTOC) of a human cell preparing to divide (G2 phase) is bleached at the position indicated by an arrow and recovery of fluorescence in the bleached spot is measured. For each of the four mitosis states, the fluorescence image is shown before, immediately after, and one second after the bleaching laser was switched on. The half time before full recovery, $t_{1/2}$, and the extent of recovery, describe the turnover of Plk1 at the MTOC. Repeated FRAP on the MTOC as the cell proceeds through mitosis reveals that the turnover of Plk1 increases dramatically as cells proceed through the early phases of mitosis. Experiment performed on DeltaVision microscope (Applied Precision) equipped with 488 nm laser. FRAP analysis software by Applied Precision. (© Dr. Catherine Lindon, University of Cambridge).

depleted. The corresponding time dependent fluorescence recovery traces for this bleached region are plotted on the far right. Here, the time constant $t_{1/2}$ denotes the time of recovery of the fluorescence signal to 50% of its value before bleaching. In the images this recovery process is seen to speed up dramatically as the cell is undergoing mitosis, going far beyond what could be explained by a free diffusion model, suggesting that the cell is taking an active role in promoting the transport of Plk1 during mitosis. Such data provide pieces in the very complex puzzle of how cells regulate themselves during their lifecycle, and what the regulating mechanisms are. For a fascinating re-

view of how proteins can travel within and between cells the reader is referred to [49].

Further fluorescence techniques are currently emerging capable of monitoring molecular transport processes within the cell, one of the most promising of which is fluorescence correlation spectroscopy (FCS) [50, 51]. Here fluorescence is observed confocally from a tiny sampling volume ($\sim 10^{-15}$ l) in the focus of a laserbeam passing through a high numerical aperture lens. If very dilute samples are used, then variations in the fluorescence signal can be observed and correlated with the underlying thermodynamic fluctuations due to Brownian motion and diffusion [52]. The fluctuations can give information on analyte mobility, changes in environmental conditions, ligand–receptor interactions, *etc.* The beauty of the technique is that the system remains in equilibrium at all times, and fluctuations around equilibrium itself are measured (in contrast to FRAP, where the system is removed far away from equilibrium, and the time for reequilibration of the system is measured). For this reason FCS may potentially be a less invasive technique. FCS is only now developing its potential through advances in technology and advances in LIF imaging, which now permits the detection of individual molecules from the sampling volume ([53]). The simple calculation shown in Sect. 3.2 shows why this is possible: individual molecules may emit tens of thousands of photons on their transit through the focal volume, resulting in detectable signal levels.

5.2 Protein–protein interactions

The previous section showed techniques for measuring molecular mobility in biochemical applications. LIF also permits the verification of molecular binding events at the live cell level. FRET (see Sect. 2.3.1) offers an exciting way of verifying protein–protein interactions. Combined with fusion protein technology this is proving to be one of the most powerful methods in the study of reaction pathways inside the living cell. For FRET the CFP (cyan fluorescent protein) and YFP (yellow fluorescent protein) variants have become a popular choice of labels, because there is a strong overlap between the emission spectrum of CFP (the donor) and the excitation spectrum of YFP (the acceptor). As stated above this is a condition for FRET to work. On the other hand, emission spectra of CFP and YFP can be discriminated from one another with little signal cross talk. For freely rotating CFP and YFP molecules (*i.e.* statistically donor and acceptor dipoles will adopt a random orientation with respect to one another), the Förster radius is about 5 nm [51]. This distance is of the order of the characteristic dimensions of many protein-protein complexes, and thus ideally suited for the study of protein interactions. In practice suspected binding partners are labelled with CFP and YFP respectively. Observation of FRET upon excitation of the donor CFP gives a strong indication that the two labelled entities interact (bind), because the r^{-6} dependence of energy transfer efficiency with distance r makes FRET observations un-

likely for noninteracting proteins. All is not as easy as it may seem though, as a proper interpretation of observed interactions by FRET requires a very careful set of controls. One pitfall is that cross excitation of the donor may be misinterpreted for FRET. In live cell environments it is very difficult to obtain a reliable set of repeatable controls, as variations in expression levels (*e.g.* number densities of fluorophores) and other parameters are difficult to control. There are many different variants of FRET to tackle such issues and the reader is referred to the literature for this [54–56]. For an excellent review on the technique consult [57]. Here we confine the discussion to one variant of FRET, namely the acceptor photobleaching method [58, 59]. It is based on the principle that if the acceptor molecules are destroyed by an intense burst of light, the energy loss rate from the donor is reduced, because the FRET decay channel disappears (see Fig. 1). As a result, fluorescence emission from the donor should increase. An advantage of the technique is that it is independent of number density in that the FRET transfer efficiency is related to the ratio of the donor fluorescence after photobleaching of the acceptor, to the donor signal before photobleaching. For FP labels this is very advantageous as expression levels in the cell can vary greatly within, and between, cells. A further advantage is that the increase in donor fluorescence is unaffected by signal bleedthrough from the acceptor molecules, as it is the acceptor that is photobleached. The FRET efficiency $\varepsilon_{\mathrm{FRET}}$ of transfer is given by:

$$\varepsilon_{\mathrm{FRET}} = 1 - F_{\mathrm{DBB}}/F_{\mathrm{DAB}} \tag{13}$$

where F_{DBB} is the donor fluorescence before bleaching and F_{DAB} is the donor fluorescence after bleaching. A disadvantage of the method is the fact that the method is not reversible once the acceptor has been bleached.

An example of this technique is shown in Fig. 8, taken from Ref. [60]. It is an elegant example of the application of FRET to visualise the regulation of transport processes across cell membranes, which are mediated by signal–receptor protein interactions. Here, the administration of cholera toxin (CTX) to live cells leads to increased binding between a transmembrane receptor protein (ERD2) in the Golgi organelle of the cell to the ARF1 protein [61]. The result of these interactions is that small transport vesicles are formed (essentially small enclosed compartments which are protected from the outside by a lipid membrane), which can carry protein cargo (in this case the cholera toxin) from the Golgi apparatus to the endoplasmatic reticulum. CTX has a domain which is recognised by ERD2, and this in turn appears to lead to an increased binding between ERD2 and ARF1 which was confirmed by FRET. ARF1 was labelled with CFP and ERD2 with YFP and FRET observed at different time intervals after administration of CTX. Fig. 8 shows the fluorescence signal obtained from the donor D (ARF1-CFP) before bleaching (top left image). The protein is seen to be located throughout the cell.

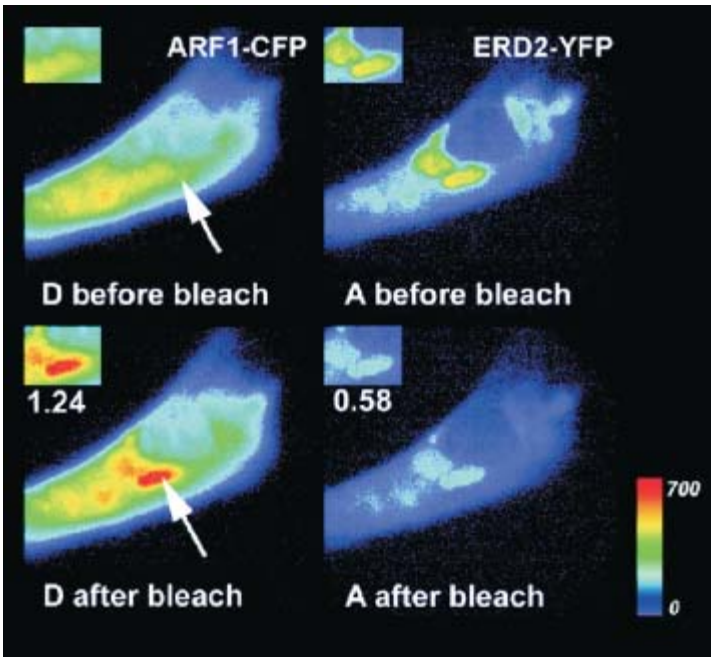

Fig. 8. FRET by acceptor photobleaching: The sequence shows how the administration of CTX (cholera toxin) can induce influence the formation of cargo vesicles which transport the toxin from the Golgi membranes. Vesicle formation is initiated by the binding of a transmembrane receptor protein in the Golgi organelles (ERD2) and the ARF1 protein. In the study, ARF1 is labelled with CFP (Donor) and ERD2 with YFP (acceptor). Upon administration of CTX a donor signal rise of 25% is observed upon photobleaching the acceptor molecules, which is not observed in the absence of CTX. The width of the insert corresponds to 10 μm. Excitation was with 800 nm using two-photon excitation of CFP and the fluorescence was observed around 485 nm for CFP and around 575 for YFP. Taken from Ref. [60]. © Elsevier 2002.

On the right the YFP signal is shown before photobleaching, signifying the location of the KDEL transmembrane receptor protein. Strong signals are obtained from the Golgi apparatus (shown in the insert), signals from the nucleus of the cell are weak. The third picture (clockwise from top left) shows the acceptor signal decrease after photobleaching. The fourth picture shows the increase in donor fluorescence after acceptor photobleaching: It is seen that there is a strong rise of ARF1-CFP signal in the Golgi apparatus by about 25% at 30 minutes after CTX was administered. Without CTX, no ARF signal increase was observed. The work confirms that physiologically meaningful studies of protein–protein interactions can be performed at the live cell level, and that the original function of the proteins is retained when labelled with CFP and YFP.

6. Conclusions

Laser induced fluorescence imaging is one of the most successful tools to investigate the dynamics of reactive systems. The power of the technique stems from the fact that it is sensitive on a large range of scales in time and in space, and, if applied sensibly, it provides a non intrusive probe, which does not change the physics or chemistry of the processes under investigation. In this article an attempt was made to convey the range of applications the technique is capable of probing, ranging from macroscopic studies of ultrafast reactions in the gas phase to the fleeting events that take place inside living cells. Variants of LIF permit the visualisation of the formation and destruction of species, of molecular transport phenomena and even the binding of individual molecules to one another. The technique's capability to provide molecular length scale information and to detect individual molecules on an almost routine basis is revolutionising the physical and biological sciences. New techniques are emerging all the time, exploiting the power of fluorescence imaging and never has the time been more exciting to work in this rich field. Concurrent with these developments, the enabling technologies are continuously improving. Novel light sources and detectors are entering the markets which are ever smaller, cheaper and more sensitive. For spectroscopists willing to look into new directions these are exciting times.

Acknowledgement

This article represents the work of a number of researchers who are gratefully acknowledged. The author is indebted to the Laser Analytics Group for their work and for proofreading the manuscript. Particular thanks go to Dr. Johan Hult, Babatunde Ayoola and Georg Hartung for provision of, and help with, figures. Special thanks are also due to Dr. Catherine Lindon of the Wellcome Trust/Cancer Research UK Gurdon Institute of Cancer and Developmental Biology for provision of Fig. 7, Dr. Irina Majoul and Prof. Rainer Duden of the School of Biological Sciences, Royal Holloway, University of London for provision of Fig. 8 – their helpful comments and discussions are much appreciated. This work has been sponsored by grants from the EC under frameworks V and VI, the Royal Society, and the EPSRC (Engineering and Physical Sciences Research Council, UK).

References

1. W. Demtröder, *Laserspektroskopie: Grundlagen und Techniken*. Springer, 4th edition (2004).
2. S. Svanberg, *Atomic and Molecular Spectroscopy*. Advanced Texts in Physics. Springer, 4th edition (2004).
3. A. C. Eckbreth, *Laser Diagnostics for Combustion Temperature and Species*, volume 3 of *Combustion Science and Technology Book Series*. Gordon and Breach, 2nd edition (1996).

4. J. R. Lakowicz, *Principles of Fluorescence Spectroscopy*. Kluwer Academic/Plenum Publishers, 2nd edition (1999).
5. M. A. Linne, *Spectroscopic Measurement: An Introduction to the Fundamentals*. Academic Press (2002).
6. K. Kohse-Höinghaus and J. B. Jeffries (eds.), *Applied Combustion Diagnostics*. Combustion: An International Series. Taylor and Francis (2002).
7. R. Kienle, M. P. Lee, and K. Kohse-Höinghaus, Appl. Phys. B **63** (1996) 403.
8. P. H. Paul, J. Phys. Chem. **99** (1995) 8472.
9. U. Rahmann, A. Bülter, U. Lenhard, R. Düsing, D. Markus, A. Brockhinke, and K. Kohse-Höinghaus, Laskin – a simulation program for time-resolved LIF-spectra. *Internal Report*. University of Bielefeld, Faculty of Chemistry, Physical Chemistry I, http://pc1.uni-bielefeld.de/∼laskin.
10. A. Bülter, U. Rahmann, K. Kohse-Höinghaus, and A. Brockhinke, Appl. Phys. B **79** (2004) 113.
11. A. Brockhinke, W. Kreutner, U. Rahmann, K. Kohse-Höinghaus, T. B. Settersten, and M. A. Linne, Appl. Phys. B **69** (1999) 477.
12. J. Daily, Prog. Energy Combust. **23** (1997) 133.
13. K. Kohse-Höinghaus, Prog. Energy Combust. Sci. **20** (1994) 203.
14. P. M. Doherty and D. R. Crosley, Appl. Opt. **23** (1984) 713.
15. A. Brockhinke and K. Kohse-Höinghaus, Faraday Discuss. **119** (2001) 275.
16. E. A. Brinkman and D. R. Crosley, J. Phys. Chem. A **108** (2004) 8084.
17. R. P. Lucht, S. Roy, and T. A. Reichardt, Prog. Energy Combust. Sci. **29** (2003) 115.
18. W. R. Ware, J. Phys. Chem. **66** (1962) 455.
19. J. R. Lakowicz and G. Weber, Biochemistry **12** (1973) 4161.
20. C. Schulz and V. Sick, Prog. Energy Combust. Science **31** (2005) 75.
21. J. B. Pawley (Ed.), *Handbook of Biological Confocal Microscopy*. Plenum Press, 2nd edition (1996).
22. T. Förster, Ann. Phys. **2** (1948) 55.
23. R. M. Clegg, Fluorescence Resonance Energy Transger. In *Fluorescence Imaging and Spectroscopy and Microscopy*, X. F. Wang and B. Herman (eds.), pp. 179–252. John Wiley & Sons, New York (1996).
24. A. Lozano, B. Yip, and R. K. Hanson, Exp. Fluids **13** (1992) 369.
25. W. Koban, J. Schorr, and C. Schulz, Appl. Phys. B **74** (2002) 111.
26. G. Herzberg, *Molecular Spectra and Molecular Structure. I. Spectra of Diatomic Molecules.* Krieger Publishing Co, Malabar (1991).
27. E. L. Winnacker *et al.* (Eds.), *Lasers in Chemistry and Biology – from the hydrogen atom to the genome* (in German), Verhandlungen der Gesellschaft Deutscher Naturforscher und Ärzte (GDNÄ), S. Hirzel Verlag Stuttgart (2001) pp. 67–82.
28. M. Oshiro and B. Moomaw, Methods Cell Biol. **72** (2003) 133.
29. J. Hynecek and T. Nishiwaki, IEEE Trans. Electron Devices **50** (2003) 239.
30. M. S. Robbins and B. J. Hadwen, IEEE Trans. Electron Devices **50** (2003) 1227.
31. S. Hell and E. H. K. Stelzer, Confocal fluorescence microscopy: Wave optics considerations and applications to cell biology. In *Visualisation in Biomedical Microscopies*, pp. 145–161. A. Kriethe (Ed.), Verlag Chemie, Weinheim (1992).
32. M. Born and E. Wolf, *Principles of Optics*. Pergamon Press, Oxford (1980).
33. R. C. Hilborn, Am. Assoc.: Phys. Teachers **50**(11) (1982) 982.
34. E. Gandin, Y. Lion, and A. van de Vorst, Photochem. Photobiol. **37** (1983) 271.
35. P. H. Paul and H. N. Najm, Proc. Combust. Inst. **27** (1998) 43.
36. C. M. Vagelopoulos and J. H. Frank, Proc. Combust. Inst. **30** (2004) 241.
37. C. M. Vagelopoulos and J. H. Frank, Proc. Combust. Inst. **29** (2002) 1721.
38. C. J. Rutland and A. Trouvé, Combust. Flame **94** (1993) 41.
39. T. Echekki and J. H. Chen, Combust. Flame **106** (1996) 184.
40. K. N. C. Bray, Proc. Combust. Inst. **26** (1996) 1.

41. W. Meier, R. S. Barlow, Y. L. Chen, and J. Y. Chen, Combust. Flame **123** (2000) 326.
42. J. Hult, U. Meier, W. Meier, A. Harvey, and C. F. Kaminski, Proc. Combust. Inst. **30** (2005) 701.
43. J. Lippincott-Schwarz and G. H. Patterson, Science **300** (2003) 87.
44. R. Y. Tsien, Annu. Rev. Biochem. **67** (1998) 509.
45. R. Heim, A. B. Cubitt, and R. Y. Tsien, Nature **373** (1995) 663.
46. E. A. J. Reits and J. J. Neefjes, Nature Cell Biol. **3** (2001) 145.
47. D. Axelrod, D. E. Koppel, J. Schlessinger, E. Elson, and W. W. Webb, Biophys. J. **16** (1976) 1055.
48. N. Periasamy and A. S. Verkman, Biophys. J. **75** (1998) 557.
49. A. J. Zhu and M. P. Scott, Genes Devel. **18** (2004) 2985.
50. E. Haustein and P. Schwille, Methods **29** (2003) 153.
51. M. A. Hink, T. Bisseling, and A. J. W. G. Visser, Plant Mol. Biol. **50** (2002) 871.
52. D. Magde, E. L. Elson, and W. W. Webb, Phys. Rev. Lett. **29** (1972) 705.
53. M. Eigen and R. Rigler, Proc. Natl. Acad. Sci. USA **91** (1994) 5740.
54. R. C. Ecker, R. de Martin, G. E. Steiner, and J. A. Schmid, Cytometry A **59** (2004) 172.
55. E. A. J. Erijman and T. Jovin, Nature Biotech. **21** (2003) 1387.
56. T. Zimmermann, J. Rietdorf, and R. Pepperkok, FEBS Lett. **546** (2003) 87.
57. C. Berney and G. Danuser, Biophys. J. **84** (2003) 3992.
58. T. Zal and N. R. J. Gascoigne, Biophys. J. **86** (2003) 3923.
59. T. S. Karpova, C. T. Baumann, L. He, X. Wu, A. Grammer, P. Lipsky, G. L. Hager, and J. G. M. C. Nally, J. Microscopy **209** (2003) 56.
60. I. Majoul, M. Straub, R. Duden, S. W. Hell, and H.-D. Söling, Rev. Mol. Biotechnol. **82** (2002) 267.
61. I. Majoul, M. Straub, S. W. Hell, R. Duden, and H.-D. Söling, Dev. Cell **1** (2001) 139, Copyright 2001 by Cell Press.